Human Molecular Genetics, 2011, Vol. 20, No. 21 ***4155–4166***
doi:10.1093/hmg/ddr339
Advance Access published on August 4, 2011

Increased hedgehog signaling in postnatal kidney results in aberrant activation of nephron developmental programs

Binghua Li[1,†], Alysha A. Rauhauser[1,†], Julie Dai[1], Ramanavelan Sakthivel[1], Peter Igarashi[1], Anton M. Jetten[3] and Massimo Attanasio[1,2,*]

[1]Department of Internal Medicine and [2]Eugene McDermott Center for Growth and Development, University of Texas Southwestern Medical Center, Dallas, TX, USA and [3]Cell Biology Section, Division of Intramural Research, National Institute of Environmental Health Sciences, National Institutes of Health, Research Triangle Park, NC, USA

Received June 28, 2011; Revised and Accepted August 1, 2011

Hedgehog (Hh) is a core signaling pathway implicated in fundamental processes during embryonic kidney development. We previously found that loss-of-function mutations in the transcription factor *GLIS2*, a putative vertebrate ortholog of *Drosophila Ci*, cause nephronophthisis type 7 in humans and mice. Kidney tubular cells in *Glis2*-knockout mice acquire mesenchymal phenotype, but the cellular mechanisms of this transition are unknown. Here, we demonstrate that Glis2 is a functional component of Hh signaling and is necessary to suppress this pathway in the postnatal kidney. In the epithelial compartment, Glis2 opposes Gli1 activity by binding *cis*-acting regulatory sequences in the 5′ flanking regions of *Snai1* and *Wnt4*, thereby inhibiting de-differentiation of tubular cells. We conclude that *Glis2* is necessary to inhibit Hh signaling and to maintain the mature tubular epithelial phenotype in the adult kidney. This is the first description of a molecular mechanism that links the Hh signaling pathway to cystic kidney diseases and can open new avenues for the treatment of diverse ciliopathies.

INTRODUCTION

Hedgehog (Hh) is a signaling pathway implicated in fundamental processes during embryonic development, including regulation of cell fate, proliferation and differentiation (1), consisting of diffusible morphogens, receptors, co-receptors and transduction factors (2). The pathway is highly conserved in the evolution, but significant differences exist between invertebrates and vertebrates, where several of the pathway's components are apparently redundant (3). Vertebrates have three Hh orthologs (Sonic, Indian and Desert) and two Patched receptors, and the functions of the intracellular effector Ci are shared among at least three proteins: Gli1, Gli2 and Gli3 (4). Gli1 exclusively and Gli2 mostly act as activators. On the other hand, full-length Gli3 is an activator of transcription but it is turned into a short repressor form by a process that requires primary cilia (5). It has been established that during kidney morphogenesis, the balance between activation and repression of the Hh pathway is determinant for the correct expression of kidney patterning genes: loss of Gli3 repressor activity results in severe defects in the number of nephrons (6,7), but the role of Hh pathway in the adult kidney has not been explored. *GLIS2* is a putative vertebrate ortholog of *Drosophila Ci*, of which loss of function results in the development of cystic kidney disease and fibrosis in humans and mice (8,9). The high sequence similarity between Glis2 and the Gli proteins together with their common localization to primary cilia led us to hypothesize that Glis2 participates in the regulation of Hh signaling in kidney tubular cells. Here, we demonstrate that Glis2 is a regulator of Hh signaling and that its repressor activity is required after birth to conclude developmental programs and maintain tubular cells in a differentiated state. These effects are at least in part obtained by the transcriptional control that Glis2 exerts on the inducer of epithelial-to-mesenchymal transition (EMT) *Snai1* and on the kidney developmental gene *Wnt4*.

*To whom correspondence should be addressed at: University of Texas Southwestern Medical Center, 5323 Harry Hines Boulevard, Dallas, TX 75390, USA. Tel: +1 2146482804; Fax: +1 2146482071; Email: massimo.attanasio@utsouthwestern.edu
†These two authors contributed equally to the work.

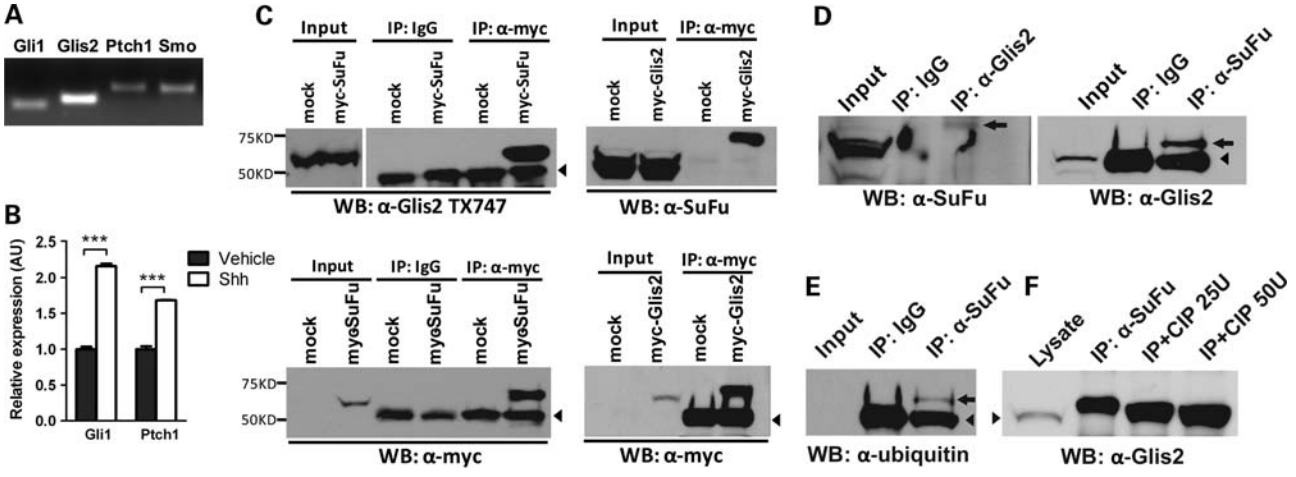

Figure 1. Glis2 is a component of the Hh signaling pathway in mouse kidneys. (**A**) RT-PCR of the components of the Hh signaling pathway in IMCD3 cells. (**B**) Expression of the Hh target genes *Gli1* and *Ptch1* is increased when IMCD3 cells are incubated in Shh-conditioned medium, as measured by real-time PCR. Error bars are SD; $^{***}P < 0.001$, $n = 3$ experiments. (**C**) Native Glis2 co-precipitates with myc-SuFu overexpressed in HEK293T cells, following immunoprecipitation with an anti-myc antibody but not with total IgG (top left). Same results are obtained when SuFu is co-precipitated with myc-Glis2 (top right). Control lysates (mock) were obtained transfecting HEK293T cells with empty myc expression vectors. The membranes were also probed with an anti-myc antibody to show the specificity of the immunoprecipitation (bottom). Arrowheads point to the IgG heavy chain band. (**D**) Reciprocal co-immunoprecipitation of endogenous Glis2 and SuFu in HEK293T lysates. Arrows indicate slower migrating proteins. Arrowhead indicates IgG heavy chains. (**E**) Western blot of endogenous HEK293T cells lysates after immunoprecipitation with an anti-SuFu antibody or total IgG as a control. Immunobloting with an anti-ubiquitin antibody shows that the precipitated complex is ubiquitinated (arrow). Arrowhead indicates IgG heavy chains. (**F**) Western blot of endogenous HEK293T cells lysates after immunoprecipitation with an anti-SuFu antibody before (IP) and after digestion with 25 or 50 U of CIP (IP+CIP). The shift in the molecular weight indicates that the Glis2 fraction immunoprecipitated with SuFu is subject to phosphorylation. Arrowhead indicates constitutive Glis2.

RESULTS

Glis2 is a functional component of the Hh signaling pathway

We performed semi-quantitative RT-PCR on mouse inner medullary collecting duct cells (IMCD3). mRNA transcripts encoding *Glis2*, *Gli1*, *Ptch1* and *Smo* were abundant in this cell line, showing that IMCD3 cells express components of the Hh pathway (Fig. 1A). *Gli1* and *Ptch1* expression increased when IMCD3 cells were grown in the presence of sonic hedgehog (Shh)-conditioned medium (Fig. 1B), indicating that this renal epithelial cell line is responsive to Shh. Gli1, Gli2 and Gli3 mediate the intracellular transduction of Hh signaling in vertebrates (3). Their activity is regulated, among other means, by the interaction with suppressor of fused (SuFu) (10,11). We have found that Glis2, like other GLI family members (12), interacts with SuFu: native Glis2 can be co-precipitated with myc-SuFu overexpressed in HEK293T cells following immunoprecipitation with an anti-myc antibody but not by total IgG (Fig. 1C, left panels; see Materials and Methods and Supplementary Material, Fig. S1, for the description of the custom-generated anti-Glis2 antibody TX747). In the reverse reaction, constitutive SuFu co-precipitated with overexpressed myc-tagged Glis2 (Fig. 1C, right panels). To verify whether this interaction occurs in a more physiological context, we reciprocally co-precipitated endogenous Glis2 and SuFu using specific antibodies, confirming the interaction between the native proteins (Fig. 1D). We also noticed that the fraction of SuFu and Glis2 that was co-precipitated was of higher molecular weight than the fraction detected in the lysates. We tested whether the shift in molecular weight depended on post-translational modification of these proteins: an anti-ubiquitin antibody reacted with the slow migrating band, indicating that the immunoprecipitated complex is ubiquitinated (Fig. 1E). We also assayed whether Glis2 was subject to phosphorylation as other members of the Gli family: incubating the immunoprecipitate with calf intestinal phosphatase (CIP) resulted in a shift in the molecular weight of the immunoprecipitated Glis2 (Fig. 1F), indicating that the fraction of Glis2 immunoprecipitated with SuFu is phosphorylated. Interestingly, the interaction of SuFu has been recently found to also regulate the proteasome-mediated cleavage of Gli3, another member of the Gli family (13). Unfortunately, we were not able to verify whether Glis2 participates to this process because of the absence of an effective anti-Gli3 antibody.

Glis2 inhibits Gli1 activity in cultured renal epithelial cells in the postnatal kidney

Gli1 is a positive effector of Hh signaling, acting as a transcriptional activator. Gli1 recognizes specific consensus sequences (Gli-binding sequences, GBSs) in the promoters of several genes (14). We previously showed that Glis2 can compete with Gli1 for binding to a GBS in a transcriptional assay *in vitro* (8). Using lentiviral vectors, we stably expressed several different *Glis2*-targeting shRNAs, or anti-GFP shRNAs as negative controls, in IMCD3 cells. We found that *Gli1* expression is strongly upregulated when *Glis2* is suppressed in IMCD3 cells (Fig. 2A and Supplementary Material, Fig. S2), indicating that Glis2 acts as a repressor of the Hh pathway. Hh signaling orchestrates the development of embryonic kidney (6,7,15), and its activity is considerably reduced at birth when it becomes restricted to the renal medulla (15). To

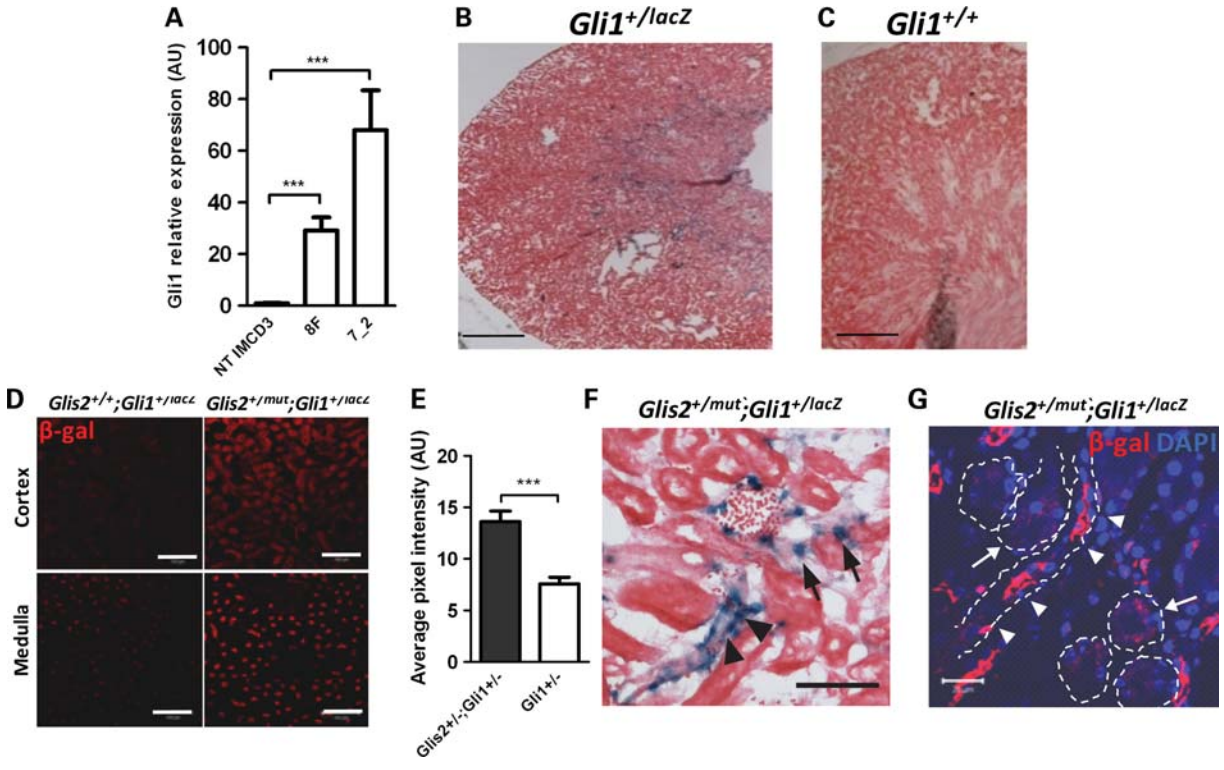

Figure 2. Glis2 represses Gli1 activity *in vitro* and *in vivo*. (**A**) *Gli1* expression in IMCD3 cells infected with retroviruses encoding non-targeting shRNA (NT) or two different shRNAs (8F and 7_2) targeting *Glis2*. Error bars are SD, $n = 3$. *** $P < 0.001$. (**B**) X-gal staining of kidneys from $Gli1^{+/lacZ}$ mice at 4 weeks after birth. β-Gal activity is present in the medulla up to the cortico-medullary junction in kidneys from $Gli1^{+/lacZ}$ mice but not from wild-type littermates (**C**); scale bar = 500 μm. (**D**) Immunofluorescence confocal microscopy of kidney cortex and medulla from $Glis2^{+/mut};Gli1^{+/lacZ}$ double-heterozygous mice and $Glis2^{+/-};Gli1^{+/lacZ}$ control littermates obtained using an anti-β-gal antibody: β-gal expression is increased in double-heterozygous kidneys. Scale = 100 μm. (**E**) Quantification of β-gal expression obtained from five independent immunofluorescence confocal microscopy images (200×), expressed as average pixel intensity. Bars are SD. ***$P < 0.001$. (**F**) X-gal staining of $Glis2^{+/mut};Gli1^{+/lacZ}$ double-heterozygous kidneys at 6 weeks after birth. β-Gal activity is mostly observed in interstitial cells (arrows) and more sparsely in some tubular compartments (arrowheads). Bar = 100 μm. (**G**) High-magnification immunofluorescence confocal image of a $Glis2^{+/mut};Gli1^{+/lacZ}$ kidney obtained using an anti β-gal antibody. Dashed lines outline longitudinal and cross-tubule sections. β-Gal (red signal) is highly expressed within structures that could represent collecting ducts (arrowheads). By immunofluorescence, β-gal expression is also observed at lower level in other tubular segments (arrows). Nuclei are stained with DAPI (blue channel). Scale bar = 20 μm.

verify whether Hh activity persists later in life, we examined β-gal expression in kidneys of $Gli1^{+/lacZ}$ mice at 4 weeks after birth. $Gli1^{+/lacZ}$ mice were generated by in-frame insertion of the *lacZ* gene after the first exon of *Gli1* and can be used as an *in vivo* readout of Hh function (16). β-Gal activity was clearly detectable in the renal medulla of $Gli1^{+/lacZ}$ mice (Fig. 2B) but not in non-transgenic controls (Fig. 2C). To exclude the possibility of an artifact, we compared the expression pattern of an unrelated gene, analyzing the kidneys of the $Sirt6^{+/lacZ}$ transgenic mouse (17). The distribution of β-gal in these two models was clearly different, with most of the signal in $Gli1^{+lacZ}$ kidneys being concentrated in the interstitium and with only few positive tubular cells (Supplementary Material, Fig. S3A–D), indicating the specificity of the reaction. As a further proof, we also tested β-gal activity in $Gli1^{+/lacZ}$ kidneys at postnatal day 1 (Supplementary Material, Fig. S3E): we found that the distribution of β-gal overlapped with the expression of another known Hh target, the gene *Ptch1*, as previously reported by others (15). All these results confirm that low levels of Hh activity are still present in the adult kidney after the development is fully completed. To verify whether Hh activity in the kidney is increased in the absence of *Glis2 in vivo*, we crossed $Glis2^{mut/mut}$ mice (18) with $Gli1^{+/lacZ}$ mice. At 4 weeks, $Glis2^{+/mut};Gli1^{+/lacZ}$ double-heterozygous mice showed significant increase of β-gal expression (Fig. 2D and E). β-Gal activity was mostly observed in interstitial cells and more sparsely in the tubular compartment (Fig. 2F). Since increased Gli1 activity results in the loss of markers of developed tubules, we could not unequivocally identify the segments expressing β-gal. The structures where the signal was more concentrated were tubules extending from the cortex to the medulla that are suggestive of collecting ducts, but β-gal was present at lower levels also in other segments (Fig. 2G).

Glis2 maintains the differentiated epithelial phenotype by inhibiting the epithelial-to-mesenchymal inducer *Snai1*

Kidney tubular cells in *Glis2*-knockout mice express markers that are characteristic of the mesenchymal lineage (8). To understand whether this phenotypic transformation is primarily due to a cell autonomous function of Glis2 in controlling cell differentiation, we further characterized the phenotype of *Glis2*-knockdown IMCD3 cells. *Glis2* suppression in this

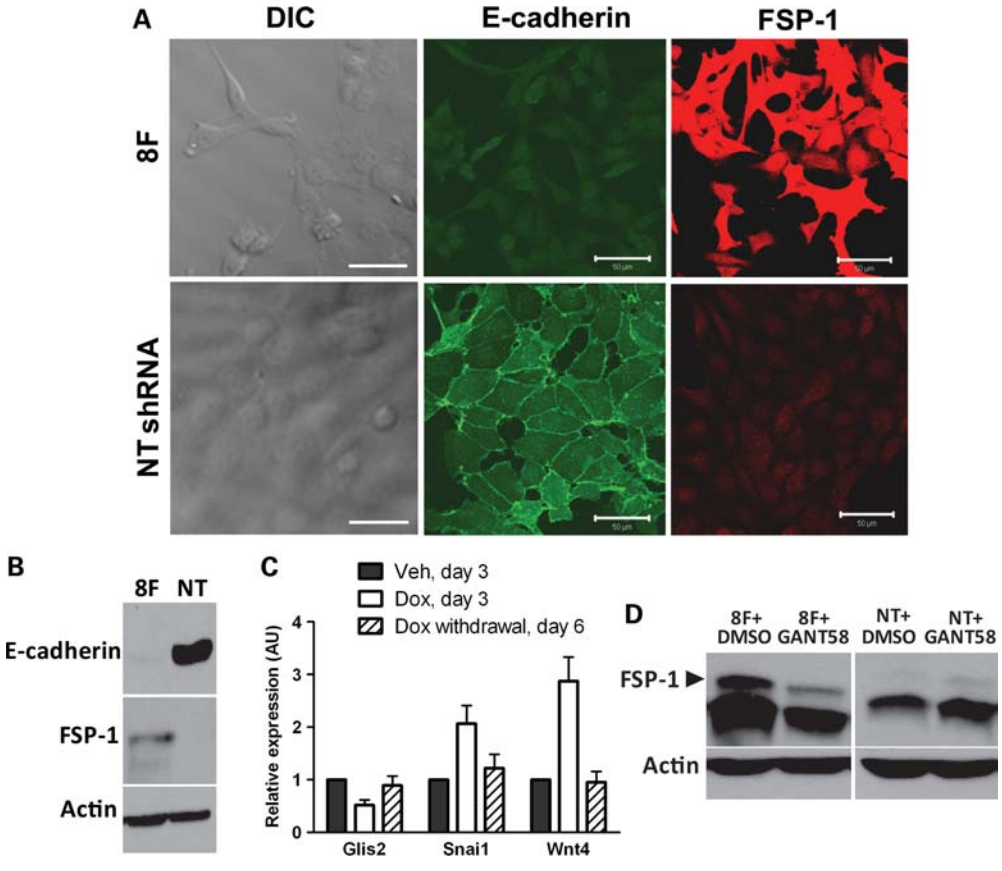

Figure 3. Glis2 maintains the differentiated tubular epithelial phenotype and inhibits the EMT-inducer *Snai1*. (**A**) *Glis2* inactivation promotes EMT in cultured IMCD3 cells. Differential interference contrast (DIC) and confocal immunofluorescence microscopy of IMCD3 cells infected with the retrovirus encoding *Glis2*-targeting shRNA (8F) or a non-targeting shRNA (NT) as a control. Inhibition of *Glis2* by shRNA results in the acquisition of mesenchymal appearance, suppression of E-cadherin and expression of FSP-1. Scale bar = 50 μm. (**B**) Differences in E-cadherin and FSP-1 protein expression detected by western blot of *Glis2*-knockdown and non-targeted IMCD3 cells used as a control. (**C**) Real-time PCR of *Snai1* and *Wnt4* in IMCD3 cells stably infected with a construct in which anti-*Glis2* shRNAs # 8 transcription was controlled by a doxycycline-inducible promoter. Cells were exposed to the vehicle (Veh, filled bars), doxycycline (Dox) for 3 days (open bars) and then returned to the regular medium for an equal time (dashed bars). The increased expression observed upon *Glis2* silencing is reversed after doxycycline withdrawal. (**D**) Increased *FSP-1* expression in *Glis2*-knockdown IMCD3 cells is partially reverted by the Gli inhibitor GANT58. NT, non-targeted clones. DMSO is used as a vehicle.

cell line resulted in the acquisition of mesenchymal hallmarks. Epithelial cells lost their typical cobblestone appearance, assumed a spindle shape, lost E-cadherin expression and expressed the mesenchymal marker S100A4/FSP-1 (Fig. 3A and B). The cells also acquired migratory capacity, as shown by time-lapse imaging (Supplementary Material, Movies S1 and S2). Five different Glis2-targeting shRNAs were used to reduce the likelihood of off-target effects and all gave comparable results. Furthermore, we generated IMCD3 cells that were stably infected with constructs in which shRNA transcription was controlled by a doxycycline-inducible promoter (19). Cells were exposed to doxycycline for 3 days and then returned to regular medium for an equal time. The increased expression of two Hh target genes, *Snai1* and *Wnt4*, observed upon *Glis2* silencing was reversed after doxycycline withdrawal (Fig. 3C), indicating that the observed upregulation is consequent to *Glis2* inactivation. These data suggest that the EMT observed *in vivo* is the result of an abnormal program triggered by the lack of *Glis2* and not the consequence of organ damage. We next sought to determine whether Hh/Gli1 overactivity was responsible for this effect. Treatment of *Glis2*-knockdown IMCD3 cells with the Gli inhibitor GANT58 (20), resulted in a decrease of FSP-1 expression (Fig. 3D), indicating that EMT is driven by Gli activators.

EMT is normally observed during gastrulation, when cells migrate from the epithelial layers of the embryo to form the primitive mesenchyme (21). The reciprocal process (mesenchymal-to-epithelial transformation, MET) occurs during normal kidney development, when metanephric mesenchymal cells become epithelial and give rise to the nephron (22). Transcription factors, such as Snail, control EMT by inhibiting E-cadherin expression and inducing mesenchymal genes (23). We previously found by microarray analysis that the transcription of the EMT inducer, *Snai1*, was upregulated in kidneys from *Glis2*-knockout mice compared with wild-type controls (8). We measured *Snai1* expression in IMCD3 *Glis2*-knockdown cells and found that *Snai1* is upregulated at RNA and protein levels (Fig. 4A and B). To investigate how Glis2 affects the regulation of *Snai1* transcription, we performed chromatin immunoprecipitation (ChIP) on IMCD3 cells using the anti-Glis2 antibody TX747 or total IgG as a control. We designed primers to obtain amplicons that

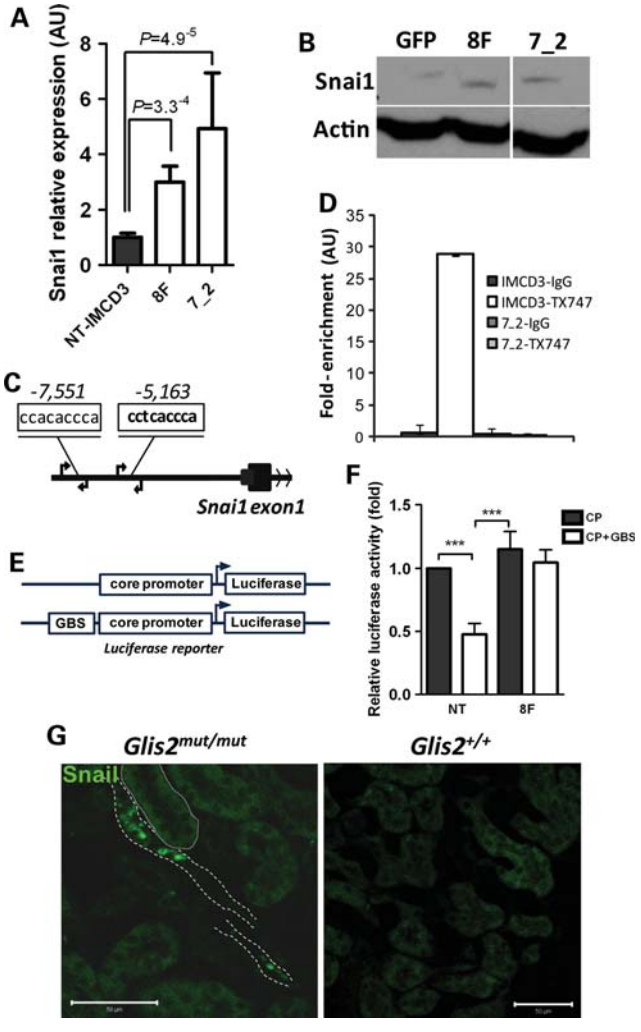

Figure 4. Glis2 binds 5′ regulatory elements and regulates the transcription of the EMT-inducer *Snai1*. Real-time PCR (**A**) and western blot analysis (**B**) of Snai1 expression in *Glis2*-knockdown IMCD3 cells (clones 8F and 7_2) compared with IMCD3 cells stably expressing a non-targeting shRNA (NT). (**C**) Schematic representation of the 5′ promoter region of the mouse *Snai1*, with two putative GBSs located at 5163 and 7551 base pairs upstream of the TTS. Arrows represent the annealing sites of the primers. (**D**) Fold enrichment of the genomic fragment containing the −5163 *cis*-regulatory element after ChIP measured by real-time PCR (AU, arbitrary units). The DNA encompassing the GBS was immunoprecipitated by the anti-Glis2 TX747 antibody but not by normal IgG. No enrichment was observed immunoprecipitating chromatin of *Glis2*-knockdown IMCD3 cells (shRNA number 7_2). Error bars are SD. $n = 3$ experiments. (**E**) Schematic representation of the reporter constructs generated for the luciferase assay. Two constructs were obtained by cloning the core promoter region of *Snai1* (above) and the −5163 GBS in front of the Snai1 core promoter (below), upstream of the firefly luciferase gene. Arrows indicate the start of the transcription of the luciferase gene. (**F**) Normalized firefly luciferase activity in *Glis2*-knockdown and control IMCD cells transfected with *Snai1* core promoter only (CP) or the GBS and core promoter (CP+GBS) plasmids. The change in luciferase activity observed in the absence of *Glis2* (8F) is likely the effect of the residual endogenous Glis2 and is not statistically significant. Error bars are SD. $n = 3$ experiments. $^{***}P < 0.001$. (**G**) Immunofluorescence confocal microscopy of the section of *Glis2*$^{mut/mut}$ and wild-type kidney obtained using an antibody against Snail. Snail is overexpressed in *Glis2*-knockout tubules reminiscent of collecting ducts (large dash) but not in structures resembling proximal/distal tubules (fine dash).

covered putative GBSs identified in the genomic sequence upstream of the *Snai1* translation start site (TSS) and tested the enrichment in the chromatin immunoprecipitated by the anti-Glis2 TX747 antibody compared with total IgG in both wild-type and knockdown IMCD3 cells. An amplicon covering a GBS located 5163 base pairs upstream of *Snai1* TSS (Fig. 4C and Supplementary Material, Table S1), but not another possible site located 2388 base pairs upstream of this sequence (not shown), was significantly enriched in chromatin from wild-type IMCD3 cells immunoprecipitated by the TX747 anti-Glis2 antibody but not by control IgG (Fig. 4D and Supplementary Material, Fig. S4A). Importantly, no enrichment was detected with ChIP assays performed when *Glis2* expression was silenced (IMCD3 7_2). To test whether this element affects the transcription of *Snai1*, we built two reporter vectors cloning the *Snai1* core promoter alone or the core promoter preceded by the −5163 GBS, upstream of the firefly luciferase gene (Fig. 4E). Luciferase activity was significantly reduced in the presence of the GBS (Fig. 4F). To confirm that lack of Glis2 results in increased *Snai1* expression also *in vivo*, we examined kidneys of Glis2$^{mut/mut}$ mice using an anti-Snail-specific antibody and we found that *Snai1* was expressed in straight tubular structures, with a distribution similar to what we observed for β-gal, in Glis2-knockout kidneys, compared with controls (Fig. 4G). Expression of *Snai1* is known to increase under conditions of *Gli1* overactivity (24). Our data indicate that Glis2 exerts a negative feedback on *Snai1* both indirectly, by inhibiting *Gli1* expression, and directly by interacting with specific 5′ regulatory elements (8). Collectively, these findings suggest that Hh drives the EMT observed in kidney tubular cells in the absence of Glis2 through upregulation of *Snai1*.

Glis2 represses the Hh-dependent expression of the developmental gene *Wnt4*

The abnormal persistence of embryonic developmental markers is observed in several models of cystic kidney disease (25,26). The definitive mammalian kidney (metanephro) develops as the result of the interaction between metanephric mesenchymal cells and the ureteric bud (27,28). The gene *Wnt4* is expressed in the metanephric mesenchyme that condenses to form pretubular aggregates, and is downregulated after the fusion of the nephron precursors (vesicles, comma-shaped and S-shaped bodies) with the collecting ducts that are derived from the ureteric bud (29). Microarrays showed that *Wnt4* was upregulated in kidneys of *Glis2*$^{-/-}$ mice (8,18). We found that *Wnt4* is also upregulated in expression microarrays performed on *Glis2*-knockdown IMCD3 cells compared with controls (data not shown). To further investigate the relationship between *Glis2* and *Wnt4*, we first confirmed that *Wnt4* expression is increased in *Glis2*-knockdown IMCD3 cells at protein (Fig. 5A) and mRNA level (Fig. 5B). Treatment with the Gli inhibitor GANT58 resulted in decreased Wnt4 expression, indicating that Wnt4 overexpression is mediated by Gli activators (Fig. 5C). We then asked whether, in these cell lines, Glis2 regulates *Wnt4*

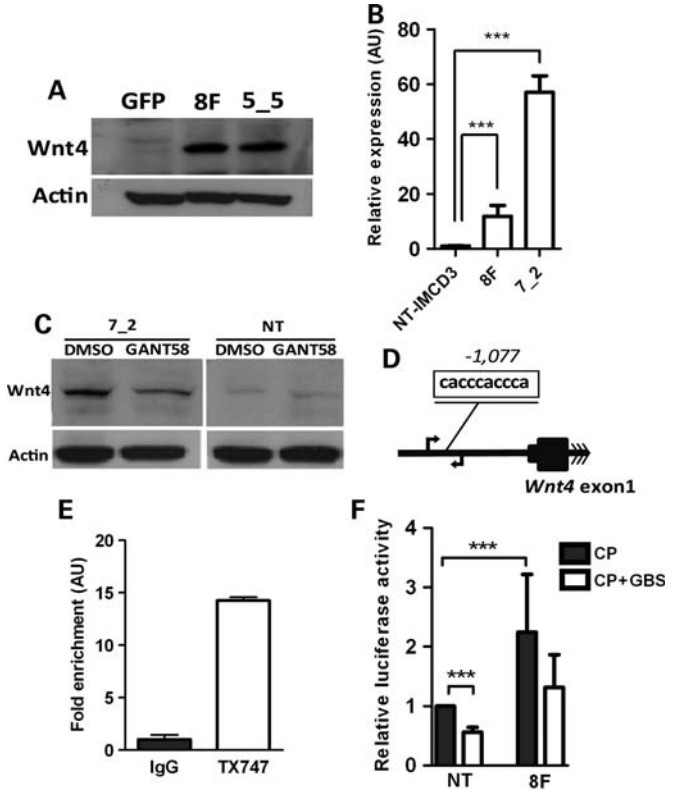

Figure 5. Glis2 binds 5′ regulatory sequences and represses *Wnt4* Hh-dependent expression. Wnt4 expression is increased at protein (**A**) and mRNA (**B**) levels in *Glis2*-knockdown IMCD3 cells. (**C**) Increased *Wnt4* expression in *Glis2*-knockdown IMCD3 cells is partially reverted by the Gli inhibitor GANT58. NT, non-targeted clones. DMSO is used as a vehicle. (**D**) Schematic representation of the genomic region upstream of *Wnt4* with the putative GBS at −1077 base pairs upstream of the TTS. Arrows indicate primer annealing sites. (**E**) Fold enrichment of the genomic fragment containing the −1077 *cis*-regulatory element after ChIP of IMCD3 cells measured by real-time PCR (AU, arbitrary units). The DNA encompassing the GBS is immunoprecipitated by the anti-Glis2 TX747 antibody but not by normal IgG. Error bars are SD. $n = 3$ experiments. (**F**) Normalized firefly luciferase activity in *Glis2*-knockdown and control IMCD cells transfected with the *Wnt4* core promoter only (CP) or the GBS plus the core promoter (CP+GBS) vector. The change in luciferase activity observed in the absence of *Glis2* (8F) is likely the effect of the residual endogenous Glis2 and is not statistically significant. Error bars are SD. $n = 3$ experiments. $^{***}P < 0.001$.

transcription. By inspecting the genomic sequence upstream of *Wnt4*, we identified a putative GBS located at −1077 base pairs from the TTS (Fig. 5D and Supplementary Material, Table S1). ChIP using the TX747 anti-Glis2 antibody resulted in the enrichment of this GBS of about 15 times, as measured by real-time PCR (Fig. 5E and Supplementary Material, Fig. S4B). When this regulatory element was cloned upstream of the core promoter of *Wnt4* (30) in a luciferase reporter vector, the transcription of the luciferase was reduced (Fig. 5F), indicating that Glis2 directly modulates *Wnt4* expression.

Wnt4 is necessary for the development of the metanephric mesenchyme (29). We hypothesized that the increased *Wnt4* expression observed in kidney tubular cell lines in the absence of *Glis2* could represent the de-differentiation of mature epithelial cells to an earlier mesenchymal stage. To test this hypothesis, we examined another developmental marker, *Pax2*, a known Hh target during kidney development (6) and found that its expression was increased in *Glis2*-knockdown IMCD3 cells but not in the non-targeted controls (Fig. 6A, lanes 2 and 4). Pax2 expression was also upregulated in *Glis2*$^{mut/mut}$ kidneys, as shown by immunofluorescence confocal microscopy (Fig. 6B and C). Treating *Glis2*-knockdown cells with GANT58 resulted in *Pax2* reduced expression, indicating that the observed effect is mediated by Gli activity (Fig. 6A, lanes 1 and 3). Taken together, these results indicate that Glis2 is an inhibitor of the Hh pathway in kidney tubular cells. Since Hh activity is downregulated after birth, we would expect Glis2 expression to rise in the kidney with the completion of the maturation. We quantified the transcription of Glis2 at several intervals after birth by real-time PCR and compared it with the expression of other Gli genes. We observed opposite expression patterns of *Glis2* compared with *Gli1*, *Gli2* and *Gli3*, at different time points after birth (Fig. 6D), suggesting that Glis2 is one of the factors that concur to the downregulation of Hh signaling in the postnatal kidney.

DISCUSSION

In this study, we have investigated the participation of *Glis2* in Hh signaling, how its absence alters this pathway and the effects that result from Hh misregulation in the postnatal kidney. The data we have presented provide for the first time evidence that *Glis2* is a repressor of the Hh pathway and that Hh/Gli signaling persists with minimal activity in fully developed kidneys. We base the conclusion that Glis2 participates in the Hh pathway on the results of biochemical and functional experiments. We show by several means that suppression of *Glis2* in cultured cells is accompanied by a significant increase of Hh activity and observe equal result *in vivo*, by using genetic crosses between the *Glis2*$^{mut/mut}$ and the Gli1^{lacZ} mouse. We report that, like other Gli proteins, Glis2 interacts with SuFu, which is an important regulator of the balance between Gli activators and repressors. Furthermore, we demonstrate that the fraction of Glis2 that is bound to SuFu is phosphorylated, whereas the immunoprecipitated Glis2-SuFu complex is subjected to ubiquitination, suggesting that the participation of Glis2 to the SuFu/Gli proteins complex (31,32) might be one of the mechanisms by which Glis2 affects the activity status of the pathway.

The data we have presented also indicate that, in the absence of *Glis2*, Hh activity abnormally persists in the kidney after the time at which the organ reaches full maturation and show that this point coincides with the peak of *Glis2* transcription after birth. The coincidence is suggestive of an important role of Glis2 in regulating the transition between developing and mature kidneys, which are characterized by high and minimal Hh activity, respectively. The nearly absent Hh signaling in the adult kidneys could be one of the reasons why the status of the pathway after birth has been virtually unexplored and that loss-of- function mutations of the important Hh activator *Gli2* do not result in kidney defects. On the other side, loss of function of *Ptch1*, a constitutive repressor of the pathway, results in the activation of Hh signaling. Embryos carrying homozygous *Ptch1* mutations die *in*

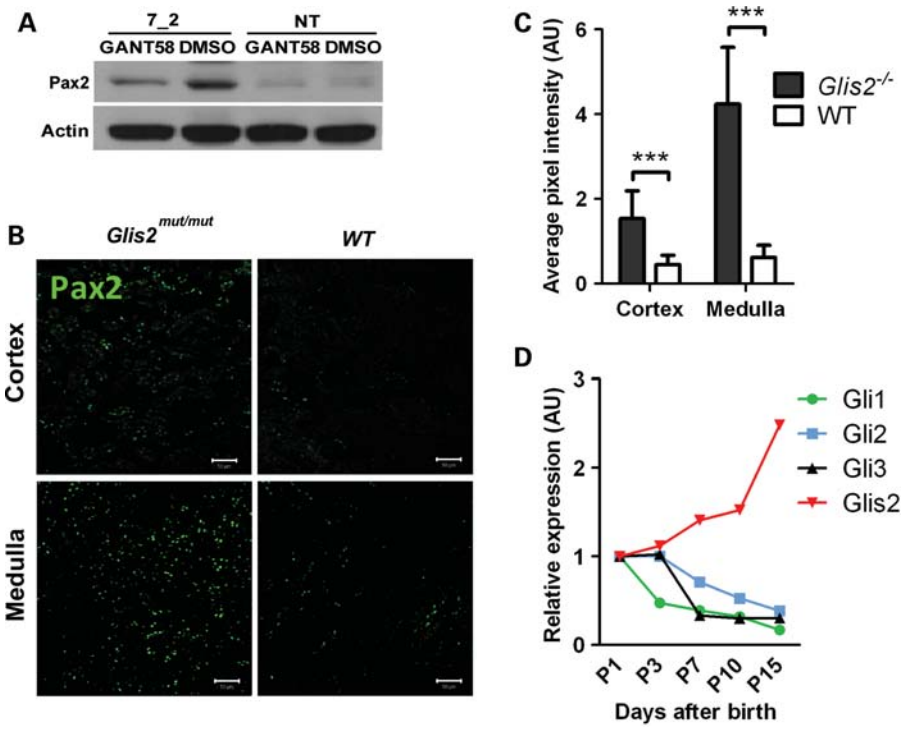

Figure 6. Pax2 is overexpressed in *Glis2*$^{mut/mut}$ kidneys. (**A**) Increased Pax2 expression in *Glis2*-knockdown IMCD3 cells is partially reverted by the Gli inhibitor GANT58. NT, non-targeted clones. DMSO was used as a vehicle. (**B**) Immunofluorescence confocal microscopy of *Glis2*$^{mut/mut}$ and wild-type kidneys: *Pax2* expression is increased in the *Glis2*$^{mut/mut}$ kidneys in both cortex (top) and medulla (bottom). Scale bar = 100 μm. (**C**) Digital quantification of the immunofluorescence in *Glis2*$^{mut/mut}$ versus wild-type kidneys calculated on 10 independent images. Error bars are SD. $^{***}P < 0.001$. (**D**) Opposite pattern of expression of *Glis2* and the other Gli proteins measured by real-time PCR in normal kidneys at five time points (days) after birth.

utero before the metanephro develops (33), but targeted inactivation of Ptch1 in the ureteric bud lineage results in renal hypoplasia secondary to ectopic activation of Hh signaling (7). Conditional inactivation of *Ptch1* after kidney development is fully reached would represent an appropriate model to verify whether withdrawal of Gli repression in a developed kidney results in the same phenotype displayed by the *Glis2*-knockout mice. The overall interpretation our results suggest that Glis2 would function by restricting Hh activity at baseline level, committing the kidney to a post-developmental state. A similar function is fulfilled by Glis2 in trigeminal ganglia, where it is necessary to promote the differentiation of postmitotic neurons from neural precursors (34), a process that is also controlled by Hh (35). This hypothesis is also concordant with a model of Hh activity gradients that establish between cortex and medulla during kidney morphogenesis (7) and might explain why an overt kidney phenotype appears only later in life in mice and humans with loss of function mutations of *Glis2*.

Distinctive characteristics of the Hh pathway in vertebrates are the partial redundancy and the numerous physical and functional interactions that exist between many components of the pathway. An example of such complex interactions is the partial functional overlap that exists between *Gli1* and *Gli2*: although homozygous inactivation of *Gli2* results in severe multi-organ malformations, *Gli1* null mutants do not have apparent phenotypes (36–38), but they develop signs of Hh deficiency (partial loss of the floor plate) when a single allele of *Gli2* is inactivated (39). This and other evidences (16) indicate that *Gli2* is the principal transcriptional regulator of Hh signaling. We think that this can explain why inactivating both *Gli1* alleles in the *Glis2* knockout does not rescue the *Glis2*$^{mut/mut}$ phenotype and we only episodically observe partial recovery of *Pax2* expression in Glis2;Gli1 double knockouts (data not shown). The mechanisms through which the abnormal Hh activation in the absence of *Glis2* results in the development of kidney cysts and fibrosis are still unclear in their integrity, but they likely include the acquisition of mesenchymal phenotype by tubular epithelial cells, implying that Hh signaling could be one of the variables that control MET during nephrogenesis. Our data regarding the role of Glis2 in Hh regulation and the physical and functional interaction of Glis2 with genomic regulatory elements of *Snai1* and *Wnt4* suggest that the MET observed in the developing kidney could be achieved through Hh-dependent regulation of genes that master the transition from mesenchymal to epithelial phenotype (*Snai1*) or are necessary to govern this process at this stage of nephrogenesis (*Wnt4* and *Pax2*). *Wnt4* and *Pax2* are required for tubule epithelialization, and their expression abruptly decreases after nephrogenesis is achieved. Our finding that loss of *Glis2* is accompanied by unscheduled expression of these genes suggests that both are required at the stage of mesenchymal condensation to promote mesenchymal differentiation into epithelial structures, but are not necessary to maintain tubules in a differentiated state. The impaired development of the kidney

observed in the absence of these genes in mice could be then ascribed to other functions, such as the control of cell survival of structures of the evolving nephron at this specific stage, which would secondarily result in a defect of tubulogenesis (40,41). Concordant with this reading are the observations that apoptosis is increased in *Pax2*-knockout mouse kidneys at this stage (40), and that IMCD3 cells undergo apoptosis after siRNA-mediated suppression of *Pax2* (41). Instead, *Pax2* overactivity, which is what we observe in our mouse model, results in the development of microcysts involving the epithelial glomerular compartment (42) that resemble the phenotype observed in *Glis2*-knockout kidneys. It would be interesting to verify whether increased apoptosis at this stage can also be detected in *Wnt4*-knockout kidneys.

The last set of considerations that arise from our experiments regards the role of primary cilia in the pathogenesis of cystic kidney diseases. It has been widely documented that most of the genes that are defective in cystic kidney diseases encode for proteins that are localized to primary cilia of renal epithelial cells (43). Similarly, disruption of Hh signaling, which, in vertebrates, is strongly dependent on cilia integrity has been repeatedly associated with cystic kidney phenotype (5,44,45). Dysregulation of some Hh target genes that we have reported in our study has also been described in humans in association with other cystic kidney diseases, as in the case of the increased expression of *Pax2* in biopsies of human subjects with NPHP (46) and autosomal dominant polycystic kidney disease (47). This observation together with the results we have presented raises the possibility that misregulation of Hh signaling could be the common determinant that leads to the development of cystic kidney disease and fibrosis in diverse forms of ciliopathies. If studies on animal models of other known ciliopathies will confirm this hypothesis, our findings could open new avenues to the therapy of cystic kidney diseases, given the availability of numerous drugs that can modulate the Hh pathway.

MATERIALS AND METHODS

Cell cultures

HEK293T (ATCC CRL-11268), SHHN293T (48) (a kind gift from Lawrence Lum, PhD, UT Southwestern Medical Center, Dallas, TX, USA) and NIH-3T3 (ATCC CRL-1658) cells were cultured at 37°C in DMEM high-glucose media (Fisher SH3002201), supplemented with 10% FBS (Fisher S11550) and 1% penicillin/streptomycin (Fisher SV30010). IMCD3 (NIH CRL-2123) cells were cultured at 37°C in DMEM F-12 media (Fisher SH3002301) supplemented with 10% FBS and 1% penicillin/streptomycin. For the Hh stimulation experiments, both purified N-terminal Shh peptide (R&D Systems, 461-SH-025) at a final concentration of 50 μM and conditioned medium from HEK293T cells stably expressing N-Shh (49) were used. Since no difference was observed between the two, all experiments were replicated using conditioned media. GANT58 (Santa Cruz, sc-221723) was added to the cell culture medium at a final concentration of 10 nM.

Mice strains

Glis2$^{mut/mut}$ mice were described somewhere else (18). *Gli1*^{lacZ} mice (16) were purchased from The Jackson Laboratory (strain #008211).

Generation of anti-Glis2 antibodies

Since commercially available antibodies had not been effective in detecting Glis2 by western blot, we generated a polyclonal antibody against the C-terminus of Glis2 (TX747, Supplementary Material, Fig. S1). To minimize possible cross-reactivity, the highly conserved Zn finger motif region was avoided in generating the antigen. A C-terminal (amino acids 318 to stop) fragment of Glis2 was cloned into 5′-6His-tagged expression vectors (pHM6G, Addgene), expressed in BL21DE3 *Escherichia coli* cells and purified by affinity chromatography using a commercial resin (Qiagen NI-NTA AGAROSE 6-His Purification). Rabbits (Covance, Immunology Services, Denver, PA, USA) were injected with 5 μg of each peptide and serum was collected after 4 weeks. Immune sera and column affinity-purified antibodies were tested for different applications. The antibody specifically recognized myc-Glis2 overexpressed in HEK293 cells and did not detect other bands in mock-transfected cells (Supplementary Material, Fig. S2a). The antibody was also effective in immunoprecipitating myc-tagged Glis2 overexpressed in HEK293T cells (Supplementary Material, Fig. S2b). We were not able to detect Glis2 in whole kidney lysates, most likely because of the low abundance of the protein.

Other antibodies

Anti-actin HRP-conjugated A3854 (Sigma); anti-β-Galactosidase 8559761 (MP Biomedicals); anti-Pax2 PRB-276P (Covance); anti-S100A4/FSP1 ab27957 (Abcam). Anti-E-Cadherin 13-1900 and Alexa Fluor® secondary antibodies A11029, A11034, A11055, A11006, A11032, A11037, A11058 and A11007 were from Invitrogen. Anti-Snai1 (sc-10432), anti-Wnt4 (sc-5214), anti-c-Myc (sc-40), bovine anti-mouse IgG-HRP (sc-2375), goat anti-rabbit IgG-HRP (sc-2054), bovine anti-goat IgG-HRP (sc-2352), goat anti-rat IgG-HRP (sc-2006), normal mouse (sc-2025), rabbit (sc-2027), goat (sc-2028) and rat (sc-2026) were from Santa Cruz.

Immunofluorescence

IMCD3 cells were cultured to 80% confluence in standard conditions. The cells were then fixed for 15 min with a 4% paraformaldheyde (PFA) solution and permeabilized for 5 min with a 0.1% Triton X-100 in PBS. Cells were blocked for 1 h with 2% goat (Fisher NC9147657) or donkey serum (Sigma D9663), probed for 2 h with primary antibody, washed five times for 5 min with PBS and probed with a secondary antibody (Invitrogen Alexa Fluor) for 1 h. Cover slips were mounted using ProLong (Invitrogen P36931). Tissues were collected after perfusion with PBS and 4% PFA and then fixed in 4% PFA for 2 h on ice. After fixing, tissues

were left in a solution of 30% sucrose in PBS at 4°C overnight, embedded in OCT compound and stored at −80°C. Tissue sections of 10 μm were air-dried for 30 min, rehydrated in PBS for 5 min, permeabilized in 0.1% Triton X-100 in PBS for 20 min and rinsed three times for 5 min in PBS. Sections were then incubated in a solution of 0.1% sodium borohydride ($NaBH_4$) for 30 min to quench autofluorescence. Sections were then rinsed with PBS and incubated in blocking solution (10% goat serum, 0.1%BSA in PBS) for 1 h at room temperature. The tissues were incubated overnight at 4°C in primary antibody diluted in blocking solution. Sections were then washed with PBS and incubated in fluorescently labeled secondary antibody diluted 1:1000 in blocking solution for 1 h at room temperature, rinsed in PBS and mounted with ProLong. Images were acquired using a Zeiss LSM 510 confocal microscope.

X-gal staining

Frozen kidney sections were fixed for 10 min with 4% PFA in PBS, washed three times for 5 min with PBS and incubated overnight in a humidified chamber at 37°C, in a solution of 1 mg/ml of X-gal. Slides were then rinsed with PBS followed by ddH_2O, counterstained with eosin and mounted with Histomount (Invitrogen).

Live-cell imaging

IMCD3 and IMCD3-Glis2KD cells (8F) were grown under normal conditions on glass-bottom tissue culture dishes (Mattek). Live-cell imaging was performed using an incubation chamber attached to a Zeiss LSM 510 confocal microscope.

Immunofluorescence quantification and image processing

Images were acquired by immunofluorescence confocal microscopy and elaborated using ImageJ software (National Institutes of Health, Bethesda, MD, USA, http://rsb.info.nih.gov/ij/). Confocal microscopy acquisition parameters (pinhole, detector and amplifier gain, amplifier offset and filters) were set using reference samples and were kept constant in the acquisition of all the remaining images. Thirty-two bit single-channel images were converted to eight-bit and the total pixel intensity, on a 256 gray-scale level, was averaged to the number of pixels.

Lentiviral vector generation and cell infection

A set of five mmu*Glis2*-targeting shRNA plasmids for lentiviral infection was purchased from Open Biosystems (RMM4534-NM_031184). The plasmid pMD.2G, encoding the broad-range VSV-G envelope, and the psPAX2 packaging plasmid were a kind gift of Dr Woodring E. Wright from the Department of Cell Biology at UT Southwestern Medical Center, Dallas, TX, USA. Calcium phosphate was used to transfect the three plasmids into HEK293T cells. Beginning 48 h after transfection, the supernatant was collected every 24 h for three times. The three samples were pooled, centrifuged for 5 min at 1500 r.p.m. and cleaned through a 0.22 μm filter. IMCD3 cells were infected at a multiplicity of infection of 0.5–1 in the presence of polybrene (8 μg/ml, Sigma, cat. H9268), and puromycin (5 μg/ml, Fisher Scientific) was added to the medium after 24 h. Twenty stably transduced clones were isolated by limiting dilution and maintained in the medium supplemented with puromycin at 2 μg/ml for 10–14 days after the infection. All procedures were compliant with the UT Southwestern Medical Center biohazard procedures.

Doxycycline-inducible Glis2-targeting shRNA expression in IMCD3 cells

We utilized the 'all-in-one' tet-on shRNA expression plasmid pLKO-Tet-On (Addgene) as described (19), to reverse the effect of Glis2 suppression in IMCD3 cells. The stuffer DNA was removed from pLKO-Tet-On by *Age*I/*Eco*RI digestion and replaced with two annealed single-stranded complementary DNA oligos (oligo sequences in Supplementary Material, Table S2). Lentivirus packaging, IMCD3 cells infection and selection were performed as described above. ShRNA expression was induced by culturing cells in the presence of 100 ng/ml doxycycline (Clontech) for the reported intervals. RNAs of Glis2 and target genes' were quantified by quantitative PCR as described below. GFP-targeting oligos were used as a negative control.

Quantitative real-time PCR

Total RNA was isolated using TRIzol (Invitrogen) and purified with Qiagen RNeasy Mini Kit according to the manufacturer's protocols. First-strand reverse transcription reactions were performed on 1 μg of total RNA using the ThermoScript RT-PCR Kit (Invitrogen). Real-time PCR were performed using iQ SYBR Green Supermix (Bio-Rad). PCR primer sequences are listed in Supplementary Material 1. Specificity of each primer pair was validated by agarose gel electrophoresis and melting curve analysis. Amplification efficiency of all primer pairs was determined by standard curve analysis of reactions performed using serial substrate dilutions. Quantification of the enrichment of *cis*-acting genomic regions was evaluated by real-time PCR as described (50). The experiments were performed on at least two independent ChIP samples and real-time PCR experiments were conducted in triplicates.

SDS–PAGE/western blotting

Protein concentrations were determined using a Pierce BCA Protein Assay Kit (PI-23225). Equal amounts of protein were mixed with 4× Laemmli sample buffer (Bio-Rad 161-0737) containing 100 mM DTT and denatured at 95°C for 10 min. Samples were run on 10% polyacrylamide gels and transferred to PVDF membranes (LC2002). After transfer, blots were blocked in 5% BSA for 2 h at room temperature or overnight at 4°C, probed with primary antibody in 1% BSA for 2 h at room temperature or overnight at 4°C, and finally probed with secondary antibody in 1% BSA for 1 h at room temperature. Antibody binding was visualized with luminol reagent (Santa Cruz, sc-2048). When necessary, blots were

stripped with 0.1 M Tris–HCL, pH 7.8, 10% SDS and 0.70% β-mercaptoethanol for 20–30 min at 50°C.

Immunoprecipitation

Cells were lysed using 0.1% Triton X-100 (Fisher AC21568-0010). Protein concentration was determined with the Pierce BCA Protein Assay Kit, and 400–600 mg of protein was used in each experiment. The lysates were pre-cleared with 50 μl of Protein A/G slurry (Santa Cruz SC-2003) for 1 h at 4°C. After centrifugation, primary antibody was added to the supernatant and incubated overnight, rotating at 4°C. One hundred microliters of protein A/G slurry was added and the samples were incubated for 1 additional hour. Beads were pelleted by centrifugation, supernatant was discarded and 2× Laemmli sample buffer containing 50 mM DTT was added to the pellet. Samples were heated at 95°C for 10 min before being run on SDS–PAGE. For assaying the phosphorylation state of Glis2, immunoprecipitates were treated with 50 U of CIP for 3 h at 37°C and loaded on gel in loading buffer.

Chromatin immunoprecipitation

About 5×10^6 wild-type IMCD3 cells and Glis2-knockdown cells (clones 8F and 7_2) were grown in 10 cm dishes. At roughly 90% confluence, the cells were rinsed with PBS and fixed with 1% formaldehyde for 10 min for crosslinking. Glycine was added to a final concentration of 125 mM for 5 min to stop the crosslinking reaction. Cells were then scraped from the dishes, spun at 2000*g* for 5 min and rinsed twice with PBS-containing protease inhibitors (PI). Cells were lysed in hypotonic buffer (5 mM PIPES, pH 8.0, 85 mM KCl, 0.5% NP-40, PI) on ice for 10 min and dounce-homogenized. Lysates were centrifuged at 10 000*g* for 10 min to pellet the nuclear fraction. The pellet was rinsed twice with hypotonic buffer before nuclear lysis (30 min on ice in 1% SDS, 10 mM EDTA, 50 mM Tris–HCl, pH 8.1, and PI). Lysates were sonicated with 8–10 s pulses and debris centrifuged at 10 000*g* for 10 min. The supernatant was removed and diluted 1:10 with ChIP dilution buffer (1% Triton X-100, 2 mM EDTA, 150 mM NaCl, 20 mM Tris–HCl, pH 8.1). Fifty microliters of protein A beads were added to preclear the lysates for 2 h at 4°C. Beads were spun down and the supernatant was removed into a new tube and incubated overnight at 4°C with 5 μg of anti-Glis2 TX747 antibody. Beads were spun down and washed as follows: 10 min with wash buffer 1 (0.1% SDS, 1% Triton X-100, 2 mM EDTA, 20 mM Tris–HCl, pH 8.1, 150 mM NaCl), 10 min with wash buffer 2 (0.1% SDS, 1% Triton X-100, 2 mM EDTA, 20 mM Tris–HCl, pH 8.1, 500 mM NaCl), 10 min with wash buffer 3 (0.25 M LiCl, 1% NP-40, 1% sodium deoxycholate, 1 mM EDTA, 10 mM Tris–HCl, pH 8.1) and two times 10 min with TE buffer. Protein–DNA complex was eluted incubating the beads in a 0.1% SDS, 0.1 M $NaHCO_3$ solution for 10 min at room temperature. Samples were then incubated in 300 mM NaCl at 65°C overnight, digested with proteinase K (45°C for 1 h) and the DNA was extracted in phenol chloroform and amplified by end-primed reaction (ChIP-Seq DNA Sample Prep Kit, Illumina).

Luciferase reporter assays

The effect of the Snai1 and Wnt4 5′ regulatory sequences on transcription was assayed using a dual-luciferase reporter system. The regulatory elements were amplified by PCR and cloned in pGL3-Basic (Promega, Inc.) upstream of the core promoter of each corresponding gene (Snai1 GBS: −5163 to −5057; Snai1 core promoter: −358 to +50. Wnt4 GBS: −1098 to −701; Wnt4 core promoter: −700 to +40). The firefly luciferase gene was placed downstream of these cassettes and used as a reporter. IMCD3-*Glis2*KD cells were co-transfected with 600 ng of these plasmids and 50 ng of a plasmid expressing Renilla luciferase. Firefly activity was assayed 48 h after transfection using a Wallac VICTOR^2 Multilabel Reader and normalized to renilla activity.

Statistics and data analysis

Error bars report standard deviation (SD). Unpaired *t*-test was used for significance testing of all the experiments. All experiments were replicated at least three times unless otherwise specified.

SUPPLEMENTARY MATERIAL

Supplementary Material is available at *HMG* online.

ACKNOWLEDGEMENTS

We would like to thank the staff of the Igarashi Laboratory for their constant technical support and Leslye Dykes for confocal microscopy assistance. *Sirt6*^{lacZ} mice were a kind gift of Roberto Coppari (UT Southwestern) and Raul Mostovslasky (Harvard Medical School, Boston). Anti-Snail antibody was kindly provided by Karl Frederick Becker (Technische Universität of Munich, Germany).

Conflict of Interest statement. None declared.

FUNDING

M.A. is supported by 2010 ASN Carl W. Gottschalk Research Scholar Grant and by NIH UT Southwestern O'Brien Kidney Research Core Center Grant (P30DK079328-04).

REFERENCES

1. Ingham, P.W. and McMahon, A.P. (2001) Hedgehog signaling in animal development: paradigms and principles. *Genes Dev.*, **15**, 3059–3087.
2. Lum, L. and Beachy, P.A. (2004) The Hedgehog response network: sensors, switches, and routers. *Science*, **304**, 1755–1759.
3. Huangfu, D. and Anderson, K.V. (2006) Signaling from Smo to Ci/Gli: conservation and divergence of Hedgehog pathways from *Drosophila* to vertebrates. *Development*, **133**, 3–14.
4. Zhang, F. and Jetten, A.M. (2001) Genomic structure of the gene encoding the human GLI-related, Kruppel-like zinc finger protein GLIS2. *Gene*, **280**, 49–57.

5. Haycraft, C.J., Banizs, B., Aydin-Son, Y., Zhang, Q., Michaud, E.J. and Yoder, B.K. (2005) Gli2 and gli3 localize to cilia and require the intraflagellar transport protein polaris for processing and function. *PLoS Genet.*, **1**, e53.
6. Hu, M.C., Mo, R., Bhella, S., Wilson, C.W., Chuang, P.T., Hui, C.C. and Rosenblum, N.D. (2006) GLI3-dependent transcriptional repression of Gli1, Gli2 and kidney patterning genes disrupts renal morphogenesis. *Development*, **133**, 569–578.
7. Cain, J.E., Islam, E., Haxho, F., Chen, L., Bridgewater, D., Nieuwenhuis, E., Hui, C.C. and Rosenblum, N.D. (2009) GLI3 repressor controls nephron number via regulation of Wnt11 and Ret in ureteric tip cells. *PLoS One*, **4**, e7313.
8. Attanasio, M., Uhlenhaut, N.H., Sousa, V.H., O'Toole, J.F., Otto, E., Anlag, K., Klugmann, C., Treier, A.C., Helou, J., Sayer, J.A. *et al.* (2007) Loss of GLIS2 causes nephronophthisis in humans and mice by increased apoptosis and fibrosis. *Nat. Genet.*, **39**, 1018–1024.
9. Zhang, F., Nakanishi, G., Kurebayashi, S., Yoshino, K., Perantoni, A., Kim, Y.S. and Jetten, A.M. (2002) Characterization of Glis2, a novel gene encoding a Gli-related, Kruppel-like transcription factor with transactivation and repressor functions. Roles in kidney development and neurogenesis. *J. Biol. Chem.*, **277**, 10139–10149.
10. Kogerman, P., Grimm, T., Kogerman, L., Krause, D., Unden, A.B., Sandstedt, B., Toftgard, R. and Zaphiropoulos, P.G. (1999) Mammalian suppressor-of-fused modulates nuclear-cytoplasmic shuttling of Gli-1. *Nat. Cell Biol.*, **1**, 312–319.
11. Merchant, M., Vajdos, F.F., Ultsch, M., Maun, H.R., Wendt, U., Cannon, J., Desmarais, W., Lazarus, R.A., de Vos, A.M. and de Sauvage, F.J. (2004) Suppressor of fused regulates Gli activity through a dual binding mechanism. *Mol. Cell. Biol.*, **24**, 8627–8641.
12. Zeruth, G.T., Yang, X.P. and Jetten, A.M. (2011) Modulation of the transactivation function and stability of Kruppel-like zinc finger protein Gli-similar 3 (Glis3) by suppressor of fused. *J. Biol. Chem.*, **286**, 22077–22089.
13. Kise, Y., Morinaka, A., Teglund, S. and Miki, H. (2009) Sufu recruits GSK3beta for efficient processing of Gli3. *Biochem. Biophys. Res. Commun.*, **387**, 569–574.
14. Yoon, J.W., Kita, Y., Frank, D.J., Majewski, R.R., Konicek, B.A., Nobrega, M.A., Jacob, H., Walterhouse, D. and Iannaccone, P. (2002) Gene expression profiling leads to identification of GLI1-binding elements in target genes and a role for multiple downstream pathways in GLI1-induced cell transformation. *J. Biol. Chem.*, **277**, 5548–5555.
15. Yu, J., Carroll, T.J. and McMahon, A.P. (2002) Sonic hedgehog regulates proliferation and differentiation of mesenchymal cells in the mouse metanephric kidney. *Development*, **129**, 5301–5312.
16. Bai, C.B., Auerbach, W., Lee, J.S., Stephen, D. and Joyner, A.L. (2002) Gli2, but not Gli1, is required for initial Shh signaling and ectopic activation of the Shh pathway. *Development*, **129**, 4753–4761.
17. Mostoslavsky, R., Chua, K.F., Lombard, D.B., Pang, W.W., Fischer, M.R., Gellon, L., Liu, P., Mostoslavsky, G., Franco, S., Murphy, M.M. *et al.* (2006) Genomic instability and aging-like phenotype in the absence of mammalian SIRT6. *Cell*, **124**, 315–329.
18. Kim, Y.S., Kang, H.S., Herbert, R., Beak, J.Y., Collins, J.B., Grissom, S.F. and Jetten, A.M. (2008) Kruppel-like zinc finger protein Glis2 is essential for the maintenance of normal renal functions. *Mol. Cell. Biol.*, **28**, 2358–2367.
19. Wiederschain, D., Wee, S., Chen, L., Loo, A., Yang, G., Huang, A., Chen, Y., Caponigro, G., Yao, Y.M., Lengauer, C. *et al.* (2009) Single-vector inducible lentiviral RNAi system for oncology target validation. *Cell Cycle*, **8**, 498–504.
20. Hyman, J.M., Firestone, A.J., Heine, V.M., Zhao, Y., Ocasio, C.A., Han, K., Sun, M., Rack, P.G., Sinha, S., Wu, J.J. *et al.* (2009) Small-molecule inhibitors reveal multiple strategies for Hedgehog pathway blockade. *Proc. Natl Acad. Sci. USA*, **106**, 14132–14137.
21. Hay, E.D. (2005) The mesenchymal cell, its role in the embryo, and the remarkable signaling mechanisms that create it. *Dev. Dyn.*, **233**, 706–720.
22. Saxen, L., Sariola, H. and Lehtonen, E. (1986) Sequential cell and tissue interactions governing organogenesis of the kidney. *Anat. Embryol. (Berl.)*, **175**, 1–6.
23. Cano, A., Perez-Moreno, M.A., Rodrigo, I., Locascio, A., Blanco, M.J., del Barrio, M.G., Portillo, F. and Nieto, M.A. (2000) The transcription factor snail controls epithelial-mesenchymal transitions by repressing E-cadherin expression. *Nat. Cell Biol.*, **2**, 76–83.
24. Li, X., Deng, W., Nail, C.D., Bailey, S.K., Kraus, M.H., Ruppert, J.M. and Lobo-Ruppert, S.M. (2006) Snail induction is an early response to Gli1 that determines the efficiency of epithelial transformation. *Oncogene*, **25**, 609–621.
25. Eng,, E., Wilson, P., Racusen,, L.C. and Burrowe,, CR (1994) Aberrant Pax-2 expression in human autosomal dominant polycystic kidney disease (ADPKD) epithelia. *J. Am. Soc. Nephrol.*, **5**, 621.
26. Winyard, P.J.D., Risdon, R.A., Sams, V.R., Dressler, G.R. and Woolf, A.S. (1996) The PAX2 transcription factor is expressed in cystic and hyperproliferative dysplastic epithelia in human kidney malformations. *J. Clin. Invest.*, **98**, 451–459.
27. Saxen, L., Sariola, H. and Lehtonen, E. (1986) Sequential cell and tissue interactions governing organogenesis of the kidney. *Anat. Embryol.*, **175**, 1–6.
28. Reidy, K.J. and Rosenblum, N.D. (2009) Cell and molecular biology of kidney development. *Semin. Nephrol.*, **29**, 321–337.
29. Stark, K., Vainio, S., Vassileva, G. and McMahon, A.P. (1994) Epithelial transformation of metanephric mesenchyme in the developing kidney regulated by *Wnt-4*. *Nature*, **372**, 679–683.
30. Yu, H., Pask, A.J., Shaw, G. and Renfree, M.B. (2009) Comparative analysis of the mammalian WNT4 promoter. *BMC Genomics*, **10**, 416.
31. Humke, E.W., Dorn, K.V., Milenkovic, L., Scott, M.P. and Rohatgi, R. (2010) The output of Hedgehog signaling is controlled by the dynamic association between Suppressor of Fused and the Gli proteins. Genes Dev., **24**, 670–682.
32. Yue, S., Chen, Y. and Cheng, S.Y. (2009) Hedgehog signaling promotes the degradation of tumor suppressor Sufu through the ubiquitin-proteasome pathway. *Oncogene*, **28**, 492–499.
33. Goodrich, L.V., Milenkovic, L., Higgins, K.M. and Scott, M.P. (1997) Altered neural cell fates and medulloblastoma in mouse patched mutants. *Science*, **277**, 1109–1113.
34. Lamar, E., Kintner, C. and Goulding, M. (2001) Identification of NKL, a novel Gli-Kruppel zinc-finger protein that promotes neuronal differentiation. *Development*, **128**, 1335–1346.
35. Ota, M. and Ito, K. (2003) Induction of neurogenin-1 expression by sonic hedgehog: its role in development of trigeminal sensory neurons. *Dev. Dyn.* **227**, 544–551.
36. Mo, R., Freer, A.M., Zinyk, D.L., Crackower, M.A., Michaud, J., Heng, H.H., Chik, K.W., Shi, X.M., Tsui, L.C., Cheng, S.H. *et al.* (1997) Specific and redundant functions of Gli2 and Gli3 zinc finger genes in skeletal patterning and development. *Development*, **124**, 113–123.
37. Matise, M.P., Epstein, D.J., Park, H.L., Platt, K.A. and Joyner, A.L. (1998) Gli2 is required for induction of floor plate and adjacent cells, but not most ventral neurons in the mouse central nervous system. *Development*, **125**, 2759–2770.
38. Ding, Q., Motoyama, J., Gasca, S., Mo, R., Sasaki, H., Rossant, J. and Hui, C.C. (1998) Diminished Sonic hedgehog signaling and lack of floor plate differentiation in Gli2 mutant mice. *Development*, **125**, 2533–2543.
39. Park, H.L., Bai, C., Platt, K.A., Matise, M.P., Beeghly, A., Hui, C.C., Nakashima, M. and Joyner, A.L. (2000) Mouse Gli1 mutants are viable but have defects in SHH signaling in combination with a Gli2 mutation. *Development*, **127**, 1593–1605.
40. Porteous, S., Torban, E., Cho, N.P., Cunliffe, H., Chua, L., McNoe, L., Ward, T., Souza, C., Gus, P., Giugliani, R. *et al.* (2000) Primary renal hypoplasia in humans and mice with PAX2 mutations: evidence of increased apoptosis in fetal kidneys of Pax2(1Neu) +/- mutant mice. *Hum. Mol. Genet.*, **9**, 1–11.
41. Torban, E., Eccles, M.R., Favor, J. and Goodyer, P.R. (2000) PAX2 suppresses apoptosis in renal collecting duct cells. *Am. J. Pathol.*, **157**, 833–842.
42. Dressler, G.R., Wilkinson, J.E., Rothenpieler, U.W., Patterson, L.T., Williams-Simons, L. and Westphal, H. (1993) Deregulation of *Pax-2* expression in transgenic mice generates severe kidney abnormalities. *Nature*, **362**, 65–67.
43. Hildebrandt, F., Attanasio, M. and Otto, E. (2009) Nephronophthisis: disease mechanisms of a ciliopathy. *J. Am. Soc. Nephrol.*, **20**, 23–35.
44. Huangfu, D. and Anderson, K.V. (2005) Cilia and Hedgehog responsiveness in the mouse. *Proc. Natl Acad. Sci. USA*, **102**, 11325–11330.

45. Wong, S.Y., Seol, A.D., So, P.L., Ermilov, A.N., Bichakjian, C.K., Epstein, E.H. Jr, Dlugosz, A.A. and Reiter, J.F. (2009) Primary cilia can both mediate and suppress Hedgehog pathway-dependent tumorigenesis. *Nat. Med.*, **15**, 1055–1061.
46. Murer, L., Caridi, G., Della Vella, M., Montini, G., Carasi, C., Ghiggeri, G. and Zacchello, G. (2002) Expression of nuclear transcription factor PAX2 in renal biopsies of juvenile nephronophthisis. *Nephron*, **91**, 588–593.
47. Stayner, C., Iglesias, D.M., Goodyer, P.R., Ellis, L., Germino, G., Zhou, J. and Eccles, M.R. (2006) Pax2 gene dosage influences cystogenesis in autosomal dominant polycystic kidney disease. *Hum. Mol. Genet.*, **15**, 3520–3528.
48. Lum, L., Yao, S., Mozer, B., Rovescalli, A., Von Kessler, D., Nirenberg, M. and Beachy, P.A. (2003) Identification of Hedgehog pathway components by RNAi in *Drosophila* cultured cells. *Science*, **299**, 2039–2045.
49. Taipale, J., Chen, J.K., Cooper, M.K., Wang, B., Mann, R.K., Milenkovic, L., Scott, M.P. and Beachy, P.A. (2000) Effects of oncogenic mutations in Smoothened and Patched can be reversed by cyclopamine. *Nature*, **406**, 1005–1009.
50. Bernstein, B.E., Kamal, M., Lindblad-Toh, K., Bekiranov, S., Bailey, D.K., Huebert, D.J., McMahon, S., Karlsson, E.K., Kulbokas, E.J. III, Gingeras, T.R. *et al.* (2005) Genomic maps and comparative analysis of histone modifications in human and mouse. *Cell*, **120**, 169–181.